Journal of Scientific Computing (2025) 103:33
https://doi.org/10.1007/s10915-025-02845-w

New Low-Dissipation Central-Upwind Schemes. Part II

Shaoshuai Chu[1,2] · Alexander Kurganov[3] · Ruixiao Xin[4]

Received: 9 May 2024 / Revised: 30 December 2024 / Accepted: 5 February 2025

Abstract
The low-dissipation central-upwind (LDCU) schemes have been recently introduced in [A. Kurganov and R. Xin, J. Sci. Comput., 96 (2023), Paper No. 56] as a modification of the central-upwind (CU) schemes from [A. Kurganov and C. T. Lin, Commun. Comput. Phys., 2 (2007), pp. 141- 163]. The LDCU schemes achieve much higher resolution of contact waves and many (two-dimensional) structures resulting from complicated wave interaction. However, the LDCU schemes sometimes produce more oscillatory results compared with the CU schemes, especially near the computational domain boundaries. In this paper, we propose a very simple—yet systematic—modification of the LDCU schemes, which completely eliminates the aforementioned oscillations almost without affecting the quality of the computed solution. This is achieved with the help of a more accurate projection step, which takes into account a possible position of the contact wave in the case such wave travels through the boundaries.

Keywords Hyperbolic systems of conservation laws · Low-dissipation central-upwind schemes · Euler equations of gas dynamics

Mathematics Subject Classification 76M12 · 65M08 · 76N15 · 35L65 · 35L67

✉ Ruixiao Xin
12331009@mail.sustech.edu.cn

Shaoshuai Chu
chu@igpm.rwth-aachen.de

Alexander Kurganov
alexander@sustech.edu.cn

[1] Department of Mathematics, RWTH Aachen University, 52056 Aachen, Germany

[2] Department of Mathematics, Shenzhen International Center for Mathematics, Southern University of Science and Technology, Shenzhen 518055, China

[3] Department of Mathematics, Shenzhen International Center for Mathematics, and Guangdong Provincial Key Laboratory of Computational Science and Material Design, Southern University of Science and Technology, Shenzhen 518055, China

[4] Department of Mathematics, Southern University of Science and Technology, Shenzhen 518055, China

Published online: 12 March 2025

1 Introduction

We consider hyperbolic systems of conservation laws, which in the one-dimensional (1-D) case read as

$$\boldsymbol{U}_t + \boldsymbol{F}(\boldsymbol{U})_x = \boldsymbol{0}, \tag{1.1}$$

and in the two-dimensional (2-D) case read as

$$\boldsymbol{U}_t + \boldsymbol{F}(\boldsymbol{U})_x + \boldsymbol{G}(\boldsymbol{U})_y = \boldsymbol{0}, \tag{1.2}$$

where x and y are spatial variables, t is the time, $\boldsymbol{U} \in \mathbb{R}^d$ is a vector of unknowns, and $\boldsymbol{F}$ and $\boldsymbol{G}$ are the x- and y-directional fluxes, respectively.

We focus on finite-volume central-upwind (CU) schemes, which were introduced in [6, 8, 9] as a "black-box" solver for general hyperbolic systems (1.1) and (1.2). Even though the CU schemes are quite accurate, efficient, and robust for a wide variety of hyperbolic systems, higher resolution of the numerical solutions can be achieved by further reducing numerical dissipation present in the CU schemes; see, e.g., [1, 7, 10]. The low-dissipation CU (LDCU) schemes have been recently proposed in [10] as a modification of the CU scheme from [7]. The LDCU schemes achieve much higher resolution of contact waves and many (two-dimensional) structures resulting from complicated wave interaction. However, the LDCU schemes sometimes produce more oscillatory results compared with the CU schemes, especially near the computational domain boundaries.

In order to suppress these spurious oscillations, we modify both 1-D and 2-D LDCU schemes. The proposed modifications are very simple, yet systematic as they are based on a more accurate projection of the evolved solution onto the original (uniform) mesh. The new LDCU schemes are developed for the 1-D and 2-D Euler equations of gas dynamics and tested on several numerical examples. The obtained numerical results demonstrate that the new schemes contain almost the same small amount of numerical dissipation as the LDCU schemes from [10] but produce substantially "cleaner", non-oscillatory computed solutions.

2 New LDCU Schemes

We follow the derivation of the LDCU scheme in [10] and use precisely the same notation as in [10].

We cover the computational domain with the finite volume cells $C_j = [x_{j-\frac{1}{2}}, x_{j+\frac{1}{2}}]$, $j = 1, \ldots, N$, which are assumed to be uniform, that is, $x_{j+\frac{1}{2}} - x_{j-\frac{1}{2}} \equiv \Delta x$. We then assume that the solution, realized in terms of its cell averages $\overline{\boldsymbol{U}}_j^n$, is available at a certain time level $t = t^n$ and reconstruct a second-order piecewise linear interpolant $\sum_j [\overline{\boldsymbol{U}}_j^n + (\boldsymbol{U}_x)_j^n (x - x_j)] \mathcal{X}_{C_j}$, where $\mathcal{X}$ denotes the characteristic function of the corresponding intervals and $(\boldsymbol{U}_x)_j^n$ are the slopes obtained using a nonlinear limiter. In the numerical experiments reported in §3, we have used a generalized minmod limiter with the minmod parameter $\theta = 1.3$; see, e.g., [11, 13, 17, 19].

We then evaluate the local speeds of propagation $a^{\pm}_{j+\frac{1}{2}}$, introduce the corresponding points $x^n_{j+\frac{1}{2},\ell} := x_{j+\frac{1}{2}} + a^-_{j+\frac{1}{2}} \Delta t^n$ and $x^n_{j+\frac{1}{2},r} := x_{j+\frac{1}{2}} + a^+_{j+\frac{1}{2}} \Delta t^n$, and integrate the system (1.1) over the space-time control volumes consisting of the "smooth" $[x_{j-\frac{1}{2},r}, x_{j+\frac{1}{2},\ell}] \times [t^n, t^{n+1}]$ and "nonsmooth" $[x_{j+\frac{1}{2},\ell}, x_{j+\frac{1}{2},r}] \times [t^n, t^{n+1}]$ areas, where $t^{n+1} := t^n + \Delta t^n$. This way

the solution is evolved in time and upon the completion of the evolution step, we obtain the intermediate cell averages $\overline{\boldsymbol{U}}^{\,\mathrm{int}}_{j+\frac{1}{2}}$ (see [10, Eq. (2.7)]) and $\overline{\boldsymbol{U}}^{\,\mathrm{int}}_{j}$ (see [10, Eq. (2.10)]).

Next, the intermediate solution, which is realized in terms of $\{\overline{\boldsymbol{U}}^{\,\mathrm{int}}_{j}\}$ and $\{\overline{\boldsymbol{U}}^{\,\mathrm{int}}_{j+\frac{1}{2}}\}$, is projected onto the original grid. To this end, we need to construct the interpolant

$$\widetilde{\boldsymbol{U}}^{\,\mathrm{int}}(x)=\sum_j\left\{\widetilde{\boldsymbol{U}}^{\,\mathrm{int}}_{j+\frac{1}{2}}(x)\mathcal{X}_{[x_{j+\frac{1}{2},\ell},x_{j+\frac{1}{2},r}]}+\overline{\boldsymbol{U}}^{\,\mathrm{int}}_{j}\mathcal{X}_{[x_{j-\frac{1}{2},r},x_{j+\frac{1}{2},\ell}]}\right\}. \tag{2.1}$$

In order to develop the original LDCU scheme in [10], we have used

$$\widetilde{\boldsymbol{U}}^{\,\mathrm{int}}_{j+\frac{1}{2}}(x)=\begin{cases}\overline{\boldsymbol{U}}^{\,\mathrm{int,L}}_{j+\frac{1}{2}}, & x<x_{j+\frac{1}{2}},\\ \overline{\boldsymbol{U}}^{\,\mathrm{int,R}}_{j+\frac{1}{2}}, & x>x_{j+\frac{1}{2}},\end{cases} \tag{2.2}$$

where $\widetilde{\boldsymbol{U}}^{\,\mathrm{int}}_{j+\frac{1}{2}}(x)$ is discontinuous at $x=x_{j+\frac{1}{2}}$. The values $\overline{\boldsymbol{U}}^{\,\mathrm{int,L}}_{j+\frac{1}{2}}$ and $\overline{\boldsymbol{U}}^{\,\mathrm{int,R}}_{j+\frac{1}{2}}$ are determined based on the conservation requirement

$$a^+_{j+\frac{1}{2}}\,\overline{\boldsymbol{U}}^{\,\mathrm{int,R}}_{j+\frac{1}{2}}-a^-_{j+\frac{1}{2}}\,\overline{\boldsymbol{U}}^{\,\mathrm{int,L}}_{j+\frac{1}{2}}=(a^+_{j+\frac{1}{2}}-a^-_{j+\frac{1}{2}})\,\overline{\boldsymbol{U}}^{\,\mathrm{int}}_{j+\frac{1}{2}}. \tag{2.3}$$

and d additional degrees of freedom, which can be used to design an accurate projection. The way these degrees freedom are utilized depends on the problem at hand. One, however, can introduce an additional degree of freedom, which may be used to further improve the accuracy of the projection step.

2.1 Modification of the Projection Step

We propose to replace (2.2) with

$$\widetilde{\boldsymbol{U}}^{\,\mathrm{int}}_{j+\frac{1}{2}}(x)=\begin{cases}\overline{\boldsymbol{U}}^{\,\mathrm{int,L}}_{j+\frac{1}{2}}, & x<\widetilde{x}_{j+\frac{1}{2}},\\ \overline{\boldsymbol{U}}^{\,\mathrm{int,R}}_{j+\frac{1}{2}}, & x>\widetilde{x}_{j+\frac{1}{2}},\end{cases} \tag{2.4}$$

where $\widetilde{x}_{j+\frac{1}{2}}=x_{j+\frac{1}{2}}+\widetilde{u}_{j+\frac{1}{2}}\Delta t^n$ and $\widetilde{u}_{j+\frac{1}{2}}\in(a^-_{j+\frac{1}{2}},a^+_{j+\frac{1}{2}})$ represents an additional degree of freedom. The conservation requirements now give

$$(a^+_{j+\frac{1}{2}}-\widetilde{u}_{j+\frac{1}{2}})\,\overline{\boldsymbol{U}}^{\,\mathrm{int,R}}_{j+\frac{1}{2}}+(\widetilde{u}_{j+\frac{1}{2}}-a^-_{j+\frac{1}{2}})\,\overline{\boldsymbol{U}}^{\,\mathrm{int,L}}_{j+\frac{1}{2}}=(a^+_{j+\frac{1}{2}}-a^-_{j+\frac{1}{2}})\,\overline{\boldsymbol{U}}^{\,\mathrm{int}}_{j+\frac{1}{2}}; \tag{2.5}$$

compare with (2.3), which is obtained from (2.5) if $\widetilde{u}_{j+\frac{1}{2}}=0$. The modified projection step is outlined in Figure 1; compare it with [10, Fig. 3].

In order to complete the derivation of the new LDCU scheme, we need to consider a particular hyperbolic system. As in [10], we study the Euler equation of gas dynamics.

2.2 New LDCU Scheme for the 1-D Euler Equations of Gas Dynamics

The 1-D Euler equations of gas dynamics reads as (1.1) with $\boldsymbol{U}=(\rho,\rho u,E)^\top$ and $\boldsymbol{F}(\boldsymbol{U})=(\rho u,\rho u^2+p,u(E+p))^\top$, where ρ is the density, u is the velocity, p is the pressure, and E is the total energy. The system is closed using the equation of states (EOS), which is in the case of ideal gas is $p=(\gamma-1)\big[E-\frac{1}{2}\rho u^2\big]$, $\gamma=\mathrm{Const}$.

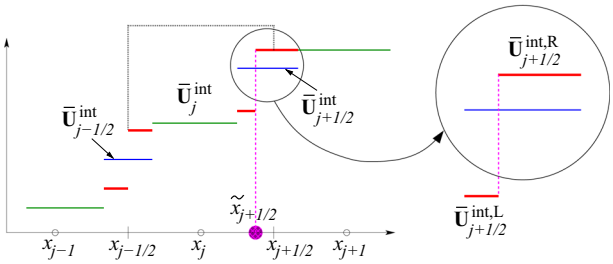

Fig. 1 A modified setting for the projection step; compare with [10, Figure 3]

In order to derive the new LDCU scheme for the 1-D Euler equations, we first follow [10, §3.1] to apply the generalized minmod reconstruction and obtain the point values $\rho^{\pm}_{j+\frac12}$, $(\rho u)^{\pm}_{j+\frac12}$, and $E^{\pm}_{j+\frac12}$, evaluate the corresponding point values $u^{\pm}_{j+\frac12}$ and $p^{\pm}_{j+\frac12}$:

$$u^{\pm}_{j+\frac12}=\frac{(\rho u)^{\pm}_{j+\frac12}}{\rho^{\pm}_{j+\frac12}},\quad p^{\pm}_{j+\frac12}=(\gamma-1)\Big[E^{\pm}_{j+\frac12}-\frac12\rho^{\pm}_{j+\frac12}\big(u^{\pm}_{j+\frac12}\big)^2\Big],$$

and estimate the one-sided local speeds of propagation $a^{\pm}_{j+\frac12}$:

$$a^{-}_{j+\frac12}=\min\Big\{u^{+}_{j+\frac12}-c^{+}_{j+\frac12},u^{-}_{j+\frac12}-c^{-}_{j+\frac12},0\Big\},\quad a^{+}_{j+\frac12}=\max\Big\{u^{+}_{j+\frac12}+c^{+}_{j+\frac12},u^{-}_{j+\frac12}+c^{-}_{j+\frac12},0\Big\}.$$

We then proceed with the evolution of the subcell averages $\overline{\boldsymbol{U}}^{\text{int,L}}_{j+\frac12}=\big(\overline{\rho}^{\text{int,L}}_{j+\frac12},(\overline{\rho u})^{\text{int,L}}_{j+\frac12},\overline{E}^{\text{int,L}}_{j+\frac12}\big)^{\top}$ and $\overline{\boldsymbol{U}}^{\text{int,R}}_{j+\frac12}=\big(\overline{\rho}^{\text{int,R}}_{j+\frac12},(\overline{\rho u})^{\text{int,R}}_{j+\frac12},\overline{E}^{\text{int,R}}_{j+\frac12}\big)^{\top}$ required in (2.4). Similarly to [10, §3], we enforce the continuity of u and p across the cell interfaces by setting

$$u^{\text{int,L}}_{j+\frac12}:=\frac{(\overline{\rho u})^{\text{int,L}}_{j+\frac12}}{\overline{\rho}^{\text{int,L}}_{j+\frac12}}=\frac{(\overline{\rho u})^{\text{int,R}}_{j+\frac12}}{\overline{\rho}^{\text{int,R}}_{j+\frac12}}=:u^{\text{int,R}}_{j+\frac12},\quad \overline{E}^{\text{int,L}}_{j+\frac12}-\frac{\big((\overline{\rho u})^{\text{int,L}}_{j+\frac12}\big)^2}{2\,\overline{\rho}^{\text{int,L}}_{j+\frac12}}=\overline{E}^{\text{int,R}}_{j+\frac12}-\frac{\big((\overline{\rho u})^{\text{int,R}}_{j+\frac12}\big)^2}{2\,\overline{\rho}^{\text{int,R}}_{j+\frac12}}. \tag{2.6}$$

Next, (2.6) together with the conservation requirement (2.5) applied to ρ, ρu, and E,

$$\begin{aligned}
(a^{+}_{j+\frac12}-\widetilde{u}_{j+\frac12})\,\overline{\rho}^{\text{int,R}}_{j+\frac12}+(\widetilde{u}_{j+\frac12}-a^{-}_{j+\frac12})\,\overline{\rho}^{\text{int,L}}_{j+\frac12}&=\big(a^{+}_{j+\frac12}-a^{-}_{j+\frac12}\big)\,\overline{\rho}^{\text{int}}_{j+\frac12},\\
(a^{+}_{j+\frac12}-\widetilde{u}_{j+\frac12})(\overline{\rho u})^{\text{int,R}}_{j+\frac12}+(\widetilde{u}_{j+\frac12}-a^{-}_{j+\frac12})(\overline{\rho u})^{\text{int,L}}_{j+\frac12}&=\big(a^{+}_{j+\frac12}-a^{-}_{j+\frac12}\big)(\overline{\rho u})^{\text{int}}_{j+\frac12},\\
(a^{+}_{j+\frac12}-\widetilde{u}_{j+\frac12})\,\overline{E}^{\text{int,R}}_{j+\frac12}+(\widetilde{u}_{j+\frac12}-a^{-}_{j+\frac12})\,\overline{E}^{\text{int,L}}_{j+\frac12}&=\big(a^{+}_{j+\frac12}-a^{-}_{j+\frac12}\big)\,\overline{E}^{\text{int}}_{j+\frac12},
\end{aligned} \tag{2.7}$$

yield a system of five algebraic equations (2.6)–(2.7), which we solve for $(\overline{\rho u})^{\text{int,L}}_{j+\frac12}$, $(\overline{\rho u})^{\text{int,R}}_{j+\frac12}$, $\overline{E}^{\text{int,L}}_{j+\frac12}$, and $\overline{E}^{\text{int,R}}_{j+\frac12}$, and express these quantities in terms of $\overline{\rho}^{\text{int,L}}_{j+\frac12}$ and $\overline{\rho}^{\text{int,R}}_{j+\frac12}$:

$$\begin{aligned}
(\overline{\rho u})^{\text{int,L}}_{j+\frac12}&=\overline{\rho}^{\text{int,L}}_{j+\frac12}u^{\text{int}}_{j+\frac12},&\qquad (\overline{\rho u})^{\text{int,R}}_{j+\frac12}&=\overline{\rho}^{\text{int,R}}_{j+\frac12}u^{\text{int}}_{j+\frac12},\\
\overline{E}^{\text{int,L}}_{j+\frac12}&=\overline{E}^{\text{int}}_{j+\frac12}+\frac{\overline{\rho}^{\text{int,L}}_{j+\frac12}-\rho^{\text{int}}_{j+\frac12}}{2}\big(u^{\text{int}}_{j+\frac12}\big)^2,&\qquad \overline{E}^{\text{int,R}}_{j+\frac12}&=\overline{E}^{\text{int}}_{j+\frac12}+\frac{\overline{\rho}^{\text{int,R}}_{j+\frac12}-\rho^{\text{int}}_{j+\frac12}}{2}\big(u^{\text{int}}_{j+\frac12}\big)^2,
\end{aligned} \tag{2.8}$$

where $u^{\text{int}}_{j+\frac{1}{2}} := (\overline{\rho u})^{\text{int}}_{j+\frac{1}{2}} / \overline{\rho}^{\text{int}}_{j+\frac{1}{2}}$.

Note that the first two equations in (2.8) give $u^{\text{int,L}}_{j+\frac{1}{2}} = u^{\text{int}}_{j+\frac{1}{2}} = u^{\text{int,R}}_{j+\frac{1}{2}}$, which suggests that in this piecewise constant solution approximation, the velocity is constant in $[x_{j+\frac{1}{2},\ell}, x_{j+\frac{1}{2},r}]$. We therefore use the same velocity value and set $\widetilde{u}_{j+\frac{1}{2}} = u^{\text{int}}_{j+\frac{1}{2}}$.

Finally, we follow the steps in [10, §3], where we make the difference $\overline{\rho}^{\text{int,R}}_{j+\frac{1}{2}} - \overline{\rho}^{\text{int,L}}_{j+\frac{1}{2}}$ as large as possible without creating any new local extrema. To this end, we denote by

$$S^-_{j+\frac{1}{2}} := (u^{\text{int}}_{j+\frac{1}{2}} - a^-_{j+\frac{1}{2}})\big(\overline{\rho}^{\text{int}}_{j+\frac{1}{2}} - \rho^{\text{int}}_{j+\frac{1}{2},\ell}\big) \quad \text{and} \quad S^+_{j+\frac{1}{2}} := (a^+_{j+\frac{1}{2}} - u^{\text{int}}_{j+\frac{1}{2}})\big(\rho^{\text{int}}_{j+\frac{1}{2},r} - \overline{\rho}^{\text{int}}_{j+\frac{1}{2}}\big), \tag{2.9}$$

where the point values $\rho^{\text{int}}_{j+\frac{1}{2},\ell}$ and $\rho^{\text{int}}_{j+\frac{1}{2},\ell}$ were introduced in [10, Eq. (2.14)], and then determine $\overline{\rho}^{\text{int,L}}_{j+\frac{1}{2}}$ and $\overline{\rho}^{\text{int,R}}_{j+\frac{1}{2}}$ by

$$\begin{aligned} \overline{\rho}^{\text{int,L}}_{j+\frac{1}{2}} &= \overline{\rho}^{\text{int}}_{j+\frac{1}{2}} + \frac{\delta_{j+\frac{1}{2}}}{a^-_{j+\frac{1}{2}} - u^{\text{int}}_{j+\frac{1}{2}}}, \\ \overline{\rho}^{\text{int,R}}_{j+\frac{1}{2}} &= \overline{\rho}^{\text{int}}_{j+\frac{1}{2}} + \frac{\delta_{j+\frac{1}{2}}}{a^+_{j+\frac{1}{2}} - u^{\text{int}}_{j+\frac{1}{2}}}, \end{aligned} \qquad \delta_{j+\frac{1}{2}} := \text{minmod}\big(S^-_{j+\frac{1}{2}}, S^+_{j+\frac{1}{2}}\big), \tag{2.10}$$

where $\text{minmod}(a,b) := \frac{1}{2}(\text{sgn}(a) + \text{sgn}(b))\min(|a|,|b|)$. We then substitute (2.10) into (2.8) and obtain

$$\begin{aligned} &(\overline{\rho u})^{\text{int,L}}_{j+\frac{1}{2}} = (\overline{\rho u})^{\text{int}}_{j+\frac{1}{2}} + \frac{\delta_{j+\frac{1}{2}}}{a^-_{j+\frac{1}{2}} - u^{\text{int}}_{j+\frac{1}{2}}} u^{\text{int}}_{j+\frac{1}{2}}, \quad (\overline{\rho u})^{\text{int,R}}_{j+\frac{1}{2}} = (\overline{\rho u})^{\text{int}}_{j+\frac{1}{2}} + \frac{\delta_{j+\frac{1}{2}}}{a^+_{j+\frac{1}{2}} - u^{\text{int}}_{j+\frac{1}{2}}} u^{\text{int}}_{j+\frac{1}{2}}, \\ &\overline{E}^{\text{int,L}}_{j+\frac{1}{2}} = \overline{E}^{\text{int}}_{j+\frac{1}{2}} + \frac{\delta_{j+\frac{1}{2}}}{2(a^-_{j+\frac{1}{2}} - u^{\text{int}}_{j+\frac{1}{2}})}\big(u^{\text{int}}_{j+\frac{1}{2}}\big)^2, \quad \overline{E}^{\text{int,R}}_{j+\frac{1}{2}} = \overline{E}^{\text{int}}_{j+\frac{1}{2}} + \frac{\delta_{j+\frac{1}{2}}}{2(a^+_{j+\frac{1}{2}} - u^{\text{int}}_{j+\frac{1}{2}})}\big(u^{\text{int}}_{j+\frac{1}{2}}\big)^2. \end{aligned} \tag{2.11}$$

Remark 2.1 Notice that compared with [10, equations (3.10), (3.14), (3.15)], $u^{\text{int}}_{j+\frac{1}{2}}$ is subtracted from $a^{\pm}_{j+\frac{1}{2}}$ in (2.9)–(2.11). This is the difference between the new and old LDCU numerical fluxes.

2.2.1 Fully Discrete Scheme

We now derive a new fully discrete LDCU scheme based on the new projection step. To this end, we integrate the piecewise constant interpolant (2.1), (2.4) over the cell C_j and obtain

$$\begin{aligned} \overline{\boldsymbol{U}}^{n+1}_j &= \overline{\boldsymbol{U}}^{\text{int}}_j + \frac{\Delta t^n}{\Delta x}\Big[a^+_{j-\frac{1}{2}}\big(\overline{\boldsymbol{U}}^{\text{int,R}}_{j-\frac{1}{2}} - \overline{\boldsymbol{U}}^{\text{int}}_j\big) - a^-_{j+\frac{1}{2}}\big(\overline{\boldsymbol{U}}^{\text{int,L}}_{j+\frac{1}{2}} - \overline{\boldsymbol{U}}^{\text{int}}_j\big) \\ &\quad + \max(u^{\text{int}}_{j-\frac{1}{2}}, 0)\big(\overline{\boldsymbol{U}}^{\text{int,L}}_{j-\frac{1}{2}} - \overline{\boldsymbol{U}}^{\text{int,R}}_{j-\frac{1}{2}}\big) - \max(u^{\text{int}}_{j+\frac{1}{2}}, 0)\big(\overline{\boldsymbol{U}}^{\text{int,L}}_{j+\frac{1}{2}} - \overline{\boldsymbol{U}}^{\text{int,R}}_{j+\frac{1}{2}}\big)\Big] \\ &\overset{(2.10),(2.11)}{=} \overline{\boldsymbol{U}}^{\text{int}}_j + \frac{\Delta t^n}{\Delta x}\Big[a^+_{j-\frac{1}{2}}\big(\overline{\boldsymbol{U}}^{\text{int}}_{j-\frac{1}{2}} - \overline{\boldsymbol{U}}^{\text{int}}_j\big) - a^-_{j+\frac{1}{2}}\big(\overline{\boldsymbol{U}}^{\text{int}}_{j+\frac{1}{2}} - \overline{\boldsymbol{U}}^{\text{int}}_j\big) + \alpha^{\text{int}}_{j-\frac{1}{2}}\boldsymbol{\delta}_{j-\frac{1}{2}} - \alpha^{\text{int}}_{j+\frac{1}{2}}\boldsymbol{\delta}_{j+\frac{1}{2}}\Big], \end{aligned} \tag{2.12}$$

where

$$\alpha^{\text{int}}_{j+\frac{1}{2}} = \begin{cases} \dfrac{a^+_{j+\frac{1}{2}}}{a^+_{j+\frac{1}{2}} - u^{\text{int}}_{j+\frac{1}{2}}} & \text{if } u^{\text{int}}_{j+\frac{1}{2}} < 0, \\ \dfrac{a^-_{j+\frac{1}{2}}}{a^-_{j+\frac{1}{2}} - u^{\text{int}}_{j+\frac{1}{2}}} & \text{otherwise,} \end{cases} \qquad \boldsymbol{\delta}_{j+\frac{1}{2}} = \delta_{j+\frac{1}{2}} \begin{pmatrix} 1 \\ u^{\text{int}}_{j+\frac{1}{2}} \\ \frac{1}{2}\left(u^{\text{int}}_{j+\frac{1}{2}}\right)^2 \end{pmatrix}. \tag{2.13}$$

2.2.2 Semi-Discrete Scheme

We now pass to the semi-discrete limit $\Delta t^n \to 0$ in (2.12)–(2.13) and proceed as in [10, §3.1.2] to end up with the following semi-discretization

$$\frac{\mathrm{d}}{\mathrm{d}t}\,\overline{\boldsymbol{U}}_j(t) = -\frac{\boldsymbol{\mathcal{F}}_{j+\frac{1}{2}}(t) - \boldsymbol{\mathcal{F}}_{j-\frac{1}{2}}(t)}{\Delta x}, \tag{2.14}$$

where $\boldsymbol{\mathcal{F}}_{j+\frac{1}{2}}$ are the modified LDCU numerical fluxes given by

$$\boldsymbol{\mathcal{F}}_{j+\frac{1}{2}} = \frac{a^+_{j+\frac{1}{2}}\boldsymbol{F}\left(\boldsymbol{U}^-_{j+\frac{1}{2}}\right) - a^-_{j+\frac{1}{2}}\boldsymbol{F}\left(\boldsymbol{U}^+_{j+\frac{1}{2}}\right)}{a^+_{j+\frac{1}{2}} - a^-_{j+\frac{1}{2}}} + \frac{a^+_{j+\frac{1}{2}}a^-_{j+\frac{1}{2}}}{a^+_{j+\frac{1}{2}} - a^-_{j+\frac{1}{2}}}\left(\boldsymbol{U}^+_{j+\frac{1}{2}} - \boldsymbol{U}^-_{j+\frac{1}{2}}\right) + \boldsymbol{q}_{j+\frac{1}{2}}, \tag{2.15}$$

and

$$\boldsymbol{q}_{j+\frac{1}{2}} = \alpha^*_{j+\frac{1}{2}} q^\rho_{j+\frac{1}{2}} \begin{pmatrix} 1 \\ u^*_{j+\frac{1}{2}} \\ \frac{1}{2}\left(u^*_{j+\frac{1}{2}}\right)^2 \end{pmatrix} \tag{2.16}$$

is a modified "built-in" anti-diffusion term with

$$\rho^*_{j+\frac{1}{2}} = \frac{a^+_{j+\frac{1}{2}}\rho^+_{j+\frac{1}{2}} - a^-_{j+\frac{1}{2}}\rho^-_{j+\frac{1}{2}} - \left[(\rho u)^+_{j+\frac{1}{2}} - (\rho u)^-_{j+\frac{1}{2}}\right]}{a^+_{j+\frac{1}{2}} - a^-_{j+\frac{1}{2}}},$$

$$(\rho u)^*_{j+\frac{1}{2}} = \frac{a^+_{j+\frac{1}{2}}(\rho u)^+_{j+\frac{1}{2}} - a^-_{j+\frac{1}{2}}(\rho u)^-_{j+\frac{1}{2}} - \left[\rho^+_{j+\frac{1}{2}}\left(u^+_{j+\frac{1}{2}}\right)^2 + p^+_{j+\frac{1}{2}} - \rho^-_{j+\frac{1}{2}}\left(u^-_{j+\frac{1}{2}}\right)^2 - p^-_{j+\frac{1}{2}}\right]}{a^+_{j+\frac{1}{2}} - a^-_{j+\frac{1}{2}}},$$

$$u^*_{j+\frac{1}{2}} = \frac{(\rho u)^*_{j+\frac{1}{2}}}{\rho^*_{j+\frac{1}{2}}}, \quad \alpha^*_{j+\frac{1}{2}} = \begin{cases} \dfrac{a^+_{j+\frac{1}{2}}}{a^+_{j+\frac{1}{2}} - u^*_{j+\frac{1}{2}}} & \text{if } u^*_{j+\frac{1}{2}} < 0, \\ \dfrac{a^-_{j+\frac{1}{2}}}{a^-_{j+\frac{1}{2}} - u^*_{j+\frac{1}{2}}} & \text{otherwise,} \end{cases}$$

$$q^\rho_{j+\frac{1}{2}} = \operatorname{minmod}\Big(\left(u^*_{j+\frac{1}{2}} - a^-_{j+\frac{1}{2}}\right)\left(\rho^*_{j+\frac{1}{2}} - \rho^-_{j+\frac{1}{2}}\right), \left(a^+_{j+\frac{1}{2}} - u^*_{j+\frac{1}{2}}\right)\left(\rho^+_{j+\frac{1}{2}} - \rho^*_{j+\frac{1}{2}}\right)\Big). \tag{2.17}$$

Note that all of the indexed quantities in (2.15)–(2.17) are time dependent, but from now on we will omit this dependence for the sake of brevity.

Remark 2.2 As in [10], the computation of numerical fluxes in (2.15) should be desingularized to avoid division by zero or very small numbers. If $a^+_{j+\frac12} < \varepsilon$ and $a^-_{j+\frac12} > -\varepsilon$ for a small positive ε, we replace the fluxes $\boldsymbol{\mathcal{F}}_{j+\frac12}$ with

$$\boldsymbol{\mathcal{F}}_{j+\frac12} = \frac{\boldsymbol{F}\big(\boldsymbol{U}^-_{j+\frac12}\big) + \boldsymbol{F}\big(\boldsymbol{U}^+_{j+\frac12}\big)}{2}.$$

In the numerical examples reported in §3, we have taken $\varepsilon = 10^{-12}$.

Remark 2.3 We would like to stress that when the developed LDCU numerical fluxes are used at the boundaries of the computational domain, a more accurate projection used in the new LDCU fluxes helps to improve the performance of the scheme near the nonreflecting (free) boundaries; see Remark 3.1 at the end of the numerical Example 1 below. When the solid wall boundary conditions are implemented using the ghost cell technique, $u^*_{j+\frac12} = 0$ at the boundary and hence, the old and new LDCU numerical fluxes coincide there. We emphasize that enforcing continuity of u at the solid wall boundary (as it is done in the projection step at every cell interface) is correct since $u^{\text{int}}_{j+\frac12} = 0$ there and setting $u^{\text{int,L}}_{j+\frac12} = u^{\text{int,R}}_{j+\frac12} = 0$ leads to the correct semi-discrete limiting value $u = 0$ at the boundary.

2.3 New LDCU Scheme for the 2-D Euler Equations of Gas Dynamics

In this section, we extend the modified semi-discrete LDCU scheme from §2.2.2 to the 2-D Euler equations of gas dynamics, which read as (1.2) with $\boldsymbol{U} = (\rho, \rho u, \rho v, E)^\top$, $\boldsymbol{F}(\boldsymbol{U}) = (\rho u, \rho u^2 + p, \rho uv, u(E+p))^\top$, and $\boldsymbol{G}(\boldsymbol{U}) = (\rho v, \rho uv, \rho v^2 + p, v(E+p))^\top$, where the notations are the same as in the 1-D case except for that now u and v are the x- and y-velocities, respectively. The system is closed using the EOS for the ideal gas $p = (\gamma-1)\big[E - \frac{\rho}{2}(u^2+v^2)\big]$.

We first introduce a uniform mesh consisting of the finite-volume cells $C_{j,k} := [x_{j-\frac12}, x_{j+\frac12}]\times[y_{k-\frac12}, y_{k+\frac12}]$ of the uniform size with $x_{j+\frac12} - x_{j-\frac12} \equiv \Delta x$ and $y_{k+\frac12} - y_{k-\frac12} \equiv \Delta y$, $j = 1, \ldots, N_x$, $k = 1, \ldots, N_y$. We assume that at certain time level t, an approximate solution, realized in terms of the cell averages $\overline{\boldsymbol{U}}_{j,k}$, is available. These cell averages are then evolved in time by solving the following system of ODEs:

$$\frac{\mathrm{d}}{\mathrm{d}t}\overline{\boldsymbol{U}}_{j,k} = -\frac{\boldsymbol{\mathcal{F}}_{j+\frac12,k} - \boldsymbol{\mathcal{F}}_{j-\frac12,k}}{\Delta x} - \frac{\boldsymbol{\mathcal{G}}_{j,k+\frac12} - \boldsymbol{\mathcal{G}}_{j,k-\frac12}}{\Delta y}, \tag{2.18}$$

where the x- and y-numerical fluxes are

$$\boldsymbol{\mathcal{F}}_{j+\frac12,k} = \frac{a^+_{j+\frac12,k}\boldsymbol{F}(\boldsymbol{U}^-_{j+\frac12,k}) - a^-_{j+\frac12,k}\boldsymbol{F}(\boldsymbol{U}^+_{j+\frac12,k})}{a^+_{j+\frac12,k} - a^-_{j+\frac12,k}} + \frac{a^+_{j+\frac12,k}a^-_{j+\frac12,k}}{a^+_{j+\frac12,k} - a^-_{j+\frac12,k}}\left(\boldsymbol{U}^+_{j+\frac12,k} - \boldsymbol{U}^-_{j+\frac12,k}\right) + \boldsymbol{q}_{j+\frac12,k}, \tag{2.19}$$

$$\boldsymbol{\mathcal{G}}_{j,k+\frac12} = \frac{b^+_{j,k+\frac12}\boldsymbol{G}(\boldsymbol{U}^-_{j,k+\frac12}) - b^-_{j,k+\frac12}\boldsymbol{G}(\boldsymbol{U}^+_{j,k+\frac12})}{b^+_{j,k+\frac12} - b^-_{j,k+\frac12}} + \frac{b^+_{j,k+\frac12}b^-_{j,k+\frac12}}{b^+_{j,k+\frac12} - b^-_{j,k+\frac12}}\left(\boldsymbol{U}^+_{j,k+\frac12} - \boldsymbol{U}^-_{j,k+\frac12}\right) + \boldsymbol{q}_{j,k+\frac12}. \tag{2.20}$$

To obtain $\boldsymbol{U}^{\pm}_{j+\frac{1}{2},k}$ and $\boldsymbol{U}^{\pm}_{j,k+\frac{1}{2}}$ in (2.19)–(2.20), we reconstruct the second-order piecewise linear interpolant $\sum_{j,k}\left[\overline{\boldsymbol{U}}_{j,k}+(\boldsymbol{U}_x)_{j,k}(x-x_j)+(\boldsymbol{U}_y)_{j,k}(y-y_k)\right]\mathcal{X}_{C_{j,k}}(x,y)$ where $(\boldsymbol{U}_x)_{j,k}$ and $(\boldsymbol{U}_y)_{j,k}$ are the slopes which are supposed to be computed using a nonlinear limiter to ensure a non-oscillatory nature of the reconstruction. In the numerical experiments reported in §3, we have used the generalized minmod limiter with the minmod parameter $\theta=1.3$. We then follow [10, §3.2] to evaluate the corresponding point values $u^{\pm}_{j+\frac{1}{2},k}$, $u^{\pm}_{j,k+\frac{1}{2}}$, $v^{\pm}_{j+\frac{1}{2},k}$, $v^{\pm}_{j,k+\frac{1}{2}}$, $p^{\pm}_{j+\frac{1}{2},k}$, and $p^{\pm}_{j,k+\frac{1}{2}}$, and estimate the one-sided local speeds of propagation $a^{\pm}_{j+\frac{1}{2},k}$ and $b^{\pm}_{j,k+\frac{1}{2}}$.

2.3.1 "Built-in" Anti-Diffusion

In this section, we discuss the derivation of the "built-in" anti-diffusion terms $\boldsymbol{q}_{j+\frac{1}{2},k}$ and $\boldsymbol{q}_{j,k+\frac{1}{2}}$ in (2.19)–(2.20) in a "dimension-by-dimension" manner following the idea introduced in [10].

In order to derive the formula for $\boldsymbol{q}_{j+\frac{1}{2},k}$, we consider the 1-D restriction of the 2-D system (1.2) along the lines $y=y_k$:

$$\boldsymbol{U}_t(x,y_k,t)+\boldsymbol{F}\big(\boldsymbol{U}(x,y_k,t)\big)_x=\boldsymbol{0},\quad k=1,\ldots,N_y. \tag{2.21}$$

We then go through all of the steps in the derivation of the 1-D fully discrete scheme for the systems in (2.21) following [10, §3.2] and §2 up to (2.4), which now reads as

$$\widetilde{\boldsymbol{U}}^{\,\mathrm{int}}_{j+\frac{1}{2},k}(x,y_k)=\begin{cases}\overline{\boldsymbol{U}}^{\,\mathrm{int,L}}_{j+\frac{1}{2},k}, & x<x_{j+\frac{1}{2}}+\widetilde{u}_{j+\frac{1}{2},k}\Delta t^n,\\ \overline{\boldsymbol{U}}^{\,\mathrm{int,R}}_{j+\frac{1}{2},k}, & x>x_{j+\frac{1}{2}}+\widetilde{u}_{j+\frac{1}{2},k}\Delta t^n,\end{cases}$$

and the corresponding local conservation requirements (2.5) become

$$\big(a^{+}_{j+\frac{1}{2},k}-\widetilde{u}_{j+\frac{1}{2},k}\big)\,\overline{\boldsymbol{U}}^{\,\mathrm{int,R}}_{j+\frac{1}{2},k}+\big(\widetilde{u}_{j+\frac{1}{2},k}-a^{-}_{j+\frac{1}{2},k}\big)\,\overline{\boldsymbol{U}}^{\,\mathrm{int,L}}_{j+\frac{1}{2},k}=\big(a^{+}_{j+\frac{1}{2},k}-a^{-}_{j+\frac{1}{2},k}\big)\,\overline{\boldsymbol{U}}^{\,\mathrm{int}}_{j+\frac{1}{2},k},$$

where we take $\widetilde{u}_{j+\frac{1}{2},k}=u^{\mathrm{int}}_{j+\frac{1}{2},k}=(\overline{\rho u})^{\mathrm{int}}_{j+\frac{1}{2},k}/\,\overline{\rho}^{\,\mathrm{int}}_{j+\frac{1}{2},k}$. We then proceed as in [10, §3.2], where we enforce the continuity of u and p across the cell interfaces $x=x_{j+\frac{1}{2}}$ by setting

$$\frac{(\overline{\rho u})^{\mathrm{int,L}}_{j+\frac{1}{2},k}}{\overline{\rho}^{\,\mathrm{int,L}}_{j+\frac{1}{2},k}}=\frac{(\overline{\rho u})^{\mathrm{int,R}}_{j+\frac{1}{2},k}}{\overline{\rho}^{\,\mathrm{int,R}}_{j+\frac{1}{2},k}},$$

$$\overline{E}^{\,\mathrm{int,L}}_{j+\frac{1}{2},k}-\frac{\big((\overline{\rho u})^{\mathrm{int,L}}_{j+\frac{1}{2},k}\big)^2+\big((\overline{\rho v})^{\mathrm{int,L}}_{j+\frac{1}{2},k}\big)^2}{2\,\overline{\rho}^{\,\mathrm{int,L}}_{j+\frac{1}{2},k}}=\overline{E}^{\,\mathrm{int,R}}_{j+\frac{1}{2},k}-\frac{\big((\overline{\rho u})^{\mathrm{int,R}}_{j+\frac{1}{2},k}\big)^2+\big((\overline{\rho v})^{\mathrm{int,R}}_{j+\frac{1}{2},k}\big)^2}{2\,\overline{\rho}^{\,\mathrm{int,R}}_{j+\frac{1}{2},k}},$$

and enforce sharp (yet, non-oscillatory) jumps of the ρ- and ρv-components. This leads to the following formulae analogous to (2.10):

$$\overline{\rho}^{\,\mathrm{int,L}}_{j+\frac{1}{2},k}=\overline{\rho}^{\,\mathrm{int}}_{j+\frac{1}{2},k}+\frac{\delta^{\rho}_{j+\frac{1}{2},k}}{a^{\mathrm{int},-}_{j+\frac{1}{2},k}},\qquad \overline{\rho}^{\,\mathrm{int,R}}_{j+\frac{1}{2},k}=\overline{\rho}^{\,\mathrm{int}}_{j+\frac{1}{2},k}+\frac{\delta^{\rho}_{j+\frac{1}{2},k}}{a^{\mathrm{int},+}_{j+\frac{1}{2},k}},$$

$$(\overline{\rho v})^{\mathrm{int,L}}_{j+\frac{1}{2},k}=(\overline{\rho v})^{\mathrm{int}}_{j+\frac{1}{2},k}+\frac{\delta^{\rho v}_{j+\frac{1}{2},k}}{a^{\mathrm{int},-}_{j+\frac{1}{2},k}},\qquad (\overline{\rho v})^{\mathrm{int,R}}_{j+\frac{1}{2},k}=(\overline{\rho v})^{\mathrm{int}}_{j+\frac{1}{2},k}+\frac{\delta^{\rho v}_{j+\frac{1}{2},k}}{a^{\mathrm{int},+}_{j+\frac{1}{2},k}},$$

where $a^{\text{int},\pm}_{j+\frac{1}{2},k} := a^{\pm}_{j+\frac{1}{2},k} - u^{\text{int}}_{j+\frac{1}{2},k}$, and

$$\delta^{\rho}_{j+\frac{1}{2},k} = \text{minmod}\left(-a^{\text{int},-}_{j+\frac{1}{2},k}\left[\overline{\rho}^{\text{int}}_{j+\frac{1}{2},k} - \left(\rho^{\text{int}}_{j+\frac{1}{2},k}\right)_{\ell}\right], a^{\text{int},+}_{j+\frac{1}{2},k}\left[\left(\rho^{\text{int}}_{j+\frac{1}{2},k}\right)_{r} - \overline{\rho}^{\text{int}}_{j+\frac{1}{2},k}\right]\right),$$

$$\delta^{\rho v}_{j+\frac{1}{2},k} = \text{minmod}\left(-a^{\text{int},-}_{j+\frac{1}{2},k}\left[(\overline{\rho v})^{\text{int}}_{j+\frac{1}{2},k} - \left((\rho v)^{\text{int}}_{j+\frac{1}{2},k}\right)_{\ell}\right], a^{\text{int},+}_{j+\frac{1}{2},k}\left[\left((\rho v)^{\text{int}}_{j+\frac{1}{2},k}\right)_{r} - (\overline{\rho v})^{\text{int}}_{j+\frac{1}{2},k}\right]\right),$$

and the point values $\left(\rho^{\text{int}}_{j+\frac{1}{2},k}\right)_{\ell}$, $\left(\rho^{\text{int}}_{j+\frac{1}{2},k}\right)_{r}$, $\left((\rho v)^{\text{int}}_{j+\frac{1}{2},k}\right)_{\ell}$, and $\left((\rho v)^{\text{int}}_{j+\frac{1}{2},k}\right)_{r}$ were introduced in [10, Eq. (2.14)].

Next, we proceed as in §2.2 and complete the derivation of the fully discrete scheme (not shown here for the sake of brevity), and after this, we pass to the semi-discrete limit and end up with the new LDCU flux (2.19) with the following "built-in" anti-diffusion term:

$$\boldsymbol{q}_{j+\frac{1}{2},k} = \alpha^{*}_{j+\frac{1}{2},k}\left(q^{\rho}_{j+\frac{1}{2},k}, u^{*}_{j+\frac{1}{2},k}q^{\rho}_{j+\frac{1}{2},k}, q^{\rho v}_{j+\frac{1}{2},k}, q^{E}_{j+\frac{1}{2},k}\right)^{\top}.$$

Here,

$$\boldsymbol{U}^{*}_{j+\frac{1}{2},k} = \frac{a^{+}_{j+\frac{1}{2},k}\boldsymbol{U}^{+}_{j+\frac{1}{2},k} - a^{-}_{j+\frac{1}{2},k}\boldsymbol{U}^{-}_{j+\frac{1}{2},k} - \left[\boldsymbol{F}(\boldsymbol{U}^{+}_{j+\frac{1}{2},k}) - \boldsymbol{F}(\boldsymbol{U}^{-}_{j+\frac{1}{2},k})\right]}{a^{+}_{j+\frac{1}{2},k} - a^{-}_{j+\frac{1}{2},k}},$$

$$u^{*}_{j+\frac{1}{2},k} = \frac{(\rho u)^{*}_{j+\frac{1}{2},k}}{\rho^{*}_{j+\frac{1}{2},k}},$$

$$q^{\rho}_{j+\frac{1}{2},k} = \text{minmod}\left(-a^{*,-}_{j+\frac{1}{2},k}\left(\rho^{*}_{j+\frac{1}{2},k} - \rho^{-}_{j+\frac{1}{2},k}\right), a^{*,+}_{j+\frac{1}{2},k}\left(\rho^{+}_{j+\frac{1}{2},k} - \rho^{*}_{j+\frac{1}{2},k}\right)\right),$$

$$q^{\rho v}_{j+\frac{1}{2},k} = \text{minmod}\left(-a^{*,-}_{j+\frac{1}{2},k}\left((\rho v)^{*}_{j+\frac{1}{2},k} - (\rho v)^{-}_{j+\frac{1}{2},k}\right), a^{*,+}_{j+\frac{1}{2},k}\left((\rho v)^{+}_{j+\frac{1}{2},k} - (\rho v)^{*}_{j+\frac{1}{2},k}\right)\right),$$

$$q^{E}_{j+\frac{1}{2},k} = \frac{a^{*,+}_{j+\frac{1}{2},k}a^{*,-}_{j+\frac{1}{2},k}}{a^{+}_{j+\frac{1}{2},k} - a^{-}_{j+\frac{1}{2},k}}\left\{\frac{\left((\rho v)^{*}_{j+\frac{1}{2},k} + \dfrac{q^{\rho v}_{j+\frac{1}{2},k}}{a^{*,+}_{j+\frac{1}{2},k}}\right)^{2}}{2\left(\rho^{*}_{j+\frac{1}{2},k} + \dfrac{q^{\rho}_{j+\frac{1}{2},k}}{a^{*,+}_{j+\frac{1}{2},k}}\right)} - \frac{\left((\rho v)^{*}_{j+\frac{1}{2},k} + \dfrac{q^{\rho v}_{j+\frac{1}{2},k}}{a^{*,-}_{j+\frac{1}{2},k}}\right)^{2}}{2\left(\rho^{*}_{j+\frac{1}{2},k} + \dfrac{q^{\rho}_{j+\frac{1}{2},k}}{a^{*,-}_{j+\frac{1}{2},k}}\right)}\right\}$$

$$+ \frac{\left(u^{*}_{j+\frac{1}{2},k}\right)^{2}}{2}q^{\rho}_{j+\frac{1}{2},k},$$

and

$$\alpha^{*}_{j+\frac{1}{2},k} = \begin{cases} \dfrac{a^{+}_{j+\frac{1}{2},k}}{a^{*,+}_{j+\frac{1}{2},k}} & \text{if } u^{*}_{j+\frac{1}{2},k} < 0, \\ \dfrac{a^{-}_{j+\frac{1}{2},k}}{a^{*,-}_{j+\frac{1}{2},k}} & \text{otherwise,} \end{cases} \qquad a^{*,\pm}_{j+\frac{1}{2},k} = a^{\pm}_{j+\frac{1}{2},k} - u^{*}_{j+\frac{1}{2},k}.$$

Similarly, the "built-in" anti-diffusion term in the new y-directional LDCU flux (2.20) is

$$\boldsymbol{q}_{j,k+\frac{1}{2}} = \alpha^{*}_{j,k+\frac{1}{2}}\left(q^{\rho}_{j,k+\frac{1}{2}}, q^{\rho u}_{j,k+\frac{1}{2}}, v^{*}_{j,k+\frac{1}{2}}q^{\rho}_{j,k+\frac{1}{2}}, q^{E}_{j,k+\frac{1}{2}}\right)^{\top}$$

with

$$\boldsymbol{U}^*_{j,k+\frac{1}{2}} = \frac{b^+_{j,k+\frac{1}{2}}\boldsymbol{U}^+_{j,k+\frac{1}{2}} - b^-_{j,k+\frac{1}{2}}\boldsymbol{U}^-_{j,k+\frac{1}{2}} - \left[\boldsymbol{G}(\boldsymbol{U}^+_{j,k+\frac{1}{2}}) - \boldsymbol{G}(\boldsymbol{U}^-_{j,k+\frac{1}{2}})\right]}{b^+_{j,k+\frac{1}{2}} - b^-_{j,k+\frac{1}{2}}},$$

$$v^*_{j,k+\frac{1}{2}} = \frac{(\rho v)^*_{j,k+\frac{1}{2}}}{\rho^*_{j,k+\frac{1}{2}}},$$

$$q^{\rho}_{j,k+\frac{1}{2}} = \text{minmod}\left(-b^{*,-}_{j,k+\frac{1}{2}}\left(\rho^*_{j,k+\frac{1}{2}} - \rho^-_{j,k+\frac{1}{2}}\right), b^{*,+}_{j,k+\frac{1}{2}}\left(\rho^+_{j,k+\frac{1}{2}} - \rho^*_{j,k+\frac{1}{2}}\right)\right),$$

$$q^{\rho u}_{j,k+\frac{1}{2}} = \text{minmod}\left(-b^{*,-}_{j,k+\frac{1}{2}}\left((\rho u)^*_{j,k+\frac{1}{2}} - (\rho u)^-_{j,k+\frac{1}{2}}\right), b^{*,+}_{j,k+\frac{1}{2}}\left((\rho u)^+_{j,k+\frac{1}{2}} - (\rho u)^*_{j,k+\frac{1}{2}}\right)\right),$$

$$q^E_{j,k+\frac{1}{2}} = \frac{b^{*,+}_{j,k+\frac{1}{2}}b^{*,-}_{j,k+\frac{1}{2}}}{b^+_{j,k+\frac{1}{2}} - b^-_{j,k+\frac{1}{2}}}\left\{\frac{\left((\rho u)^*_{j,k+\frac{1}{2}} + \dfrac{q^{\rho u}_{j,k+\frac{1}{2}}}{b^{*,+}_{j,k+\frac{1}{2}}}\right)^2}{2\left(\rho^*_{j,k+\frac{1}{2}} + \dfrac{q^{\rho}_{j,k+\frac{1}{2}}}{b^{*,+}_{j,k+\frac{1}{2}}}\right)} - \frac{\left((\rho u)^*_{j,k+\frac{1}{2}} + \dfrac{q^{\rho u}_{j,k+\frac{1}{2}}}{b^{*,-}_{j,k+\frac{1}{2}}}\right)^2}{2\left(\rho^*_{j,k+\frac{1}{2}} + \dfrac{q^{\rho}_{j,k+\frac{1}{2}}}{b^{*,-}_{j,k+\frac{1}{2}}}\right)}\right\}$$

$$+ \frac{\left(v^*_{j,k+\frac{1}{2}}\right)^2}{2}q^{\rho}_{j,k+\frac{1}{2}},$$

and

$$\alpha^*_{j,k+\frac{1}{2}} = \begin{cases} \dfrac{b^+_{j,k+\frac{1}{2}}}{b^{*,+}_{j,k+\frac{1}{2}}} & \text{if } v^*_{j,k+\frac{1}{2}} < 0, \\ \dfrac{b^-_{j,k+\frac{1}{2}}}{b^{*,-}_{j,k+\frac{1}{2}}} & \text{otherwise,} \end{cases} \qquad b^{*,\pm}_{j,k+\frac{1}{2}} = b^{\pm}_{j,k+\frac{1}{2}} - v^*_{j,k+\frac{1}{2}}.$$

Remark 2.4 As in the 1-D case, the computation of numerical fluxes in (2.19) and (2.20) should be desingularized to avoid division by zero or very small numbers:

- If $a^+_{j+\frac{1}{2},k} < \varepsilon$ and $a^-_{j+\frac{1}{2},k} > -\varepsilon$ for a small positive ε, we replace the flux $\boldsymbol{\mathcal{F}}_{j+\frac{1}{2},k}$ with

$$\boldsymbol{\mathcal{F}}_{j+\frac{1}{2},k} = \frac{\boldsymbol{F}\left(\boldsymbol{U}^-_{j+\frac{1}{2},k}\right) + \boldsymbol{F}\left(\boldsymbol{U}^+_{j+\frac{1}{2},k}\right)}{2};$$

- If $b^+_{j,k+\frac{1}{2}} < \varepsilon$ and $b^-_{j,k+\frac{1}{2}} > -\varepsilon$, we replace the flux $\boldsymbol{\mathcal{G}}_{j,k+\frac{1}{2}}$ with

$$\boldsymbol{\mathcal{G}}_{j,k+\frac{1}{2}} = \frac{\boldsymbol{G}\left(\boldsymbol{U}^-_{j,k+\frac{1}{2}}\right) + \boldsymbol{G}\left(\boldsymbol{U}^+_{j,k+\frac{1}{2}}\right)}{2}.$$

In the numerical examples reported in §3, we have taken $\varepsilon = 10^{-12}$.

3 Numerical Examples

In this section, we apply the developed schemes to several initial-boundary value problems for the 1-D and 2-D Euler equations of gas dynamics (with $\gamma = 1.4$) and compare the

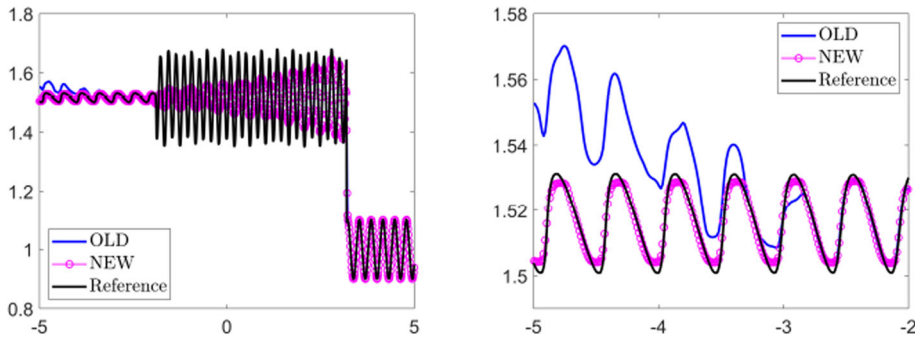

Fig. 2 Example 1: Density ρ computed by the OLD and NEW schemes (left) and zoom at $x \in [-5, -2]$ (right)

performance of the new and original second-order LDCU schemes, which will be referred to as the NEW and OLD schemes.

For time integration of the ODE systems (2.14) and (2.18), we have used the three-stage third-order strong stability preserving Runge-Kutta (SSPRK3) method (see, e.g.,[4, 5]) with the CFL number 0.475.

Example 1—Shock-Entropy Problem

In the first example taken from [16], we consider the shock-entropy wave interaction problem with the following initial condition:

$$\big(\rho(x,0),\, u(x,0),\, p(x,0)\big) = \begin{cases} (1.51695,\, 0.523346,\, 1.805), & x < -4.5, \\ (1 + 0.1\sin(20x),\, 0,\, 1), & x > -4.5, \end{cases}$$

which corresponds to a forward-facing shock wave of Mach number 1.1 interacting with high-frequency density perturbations, that is, as the shock wave moves, the perturbations spread ahead.

We compute the numerical solution using both the NEW and OLD schemes in the computational domain $[-5, 5]$ on a uniform mesh with $\Delta x = 1/80$. We impose the free boundary conditions by simply setting $\overline{\boldsymbol{U}}_0 := \overline{\boldsymbol{U}}_1$ and $\overline{\boldsymbol{U}}_{N+1} := \overline{\boldsymbol{U}}_N$ in the ghost cells C_0 and C_{N+1} on the left and on the right, respectively. The numerical results at time $t = 5$ are presented in Figure 2 along with the corresponding reference solution computed by the NEW scheme on a much finer mesh with $\Delta x = 1/800$. As one can see, the numerical solution computed by the OLD scheme is very inaccurate near the left boundary of the computational domain, while the NEW scheme accurately captures the solution throughout the entire computational domain.

Remark 3.1 It is interesting to understand the reason why the OLD scheme handles the free boundary condition in such an inaccurate way. Even though we cannot conduct a precise analysis of the boundary conditions for the studied schemes, we believe that since the cell interface coincides with the boundary of the computational domain, the computation of the numerical fluxes is affected by the piecewise constant approximation used in the projection step. While the NEW flux takes into account the speed of the flow that leaves the computational domain through the boundary, the OLD projection procedure always places the jump in the

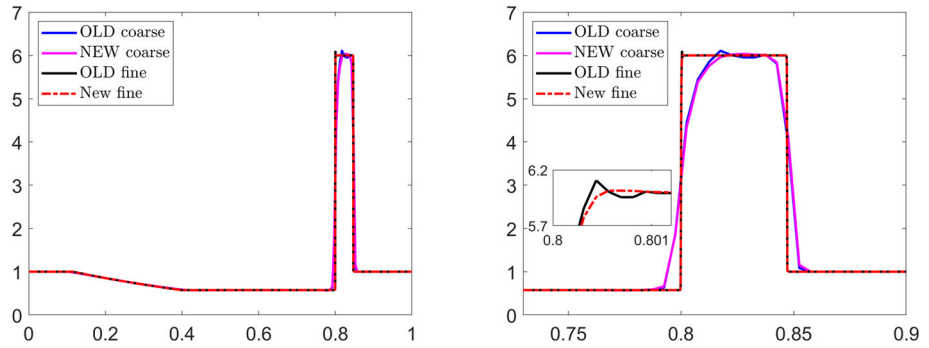

Fig. 3 Example 2: Density ρ computed by the OLD and NEW schemes on two uniform meshes (left) and zoom at $x \in [0.7, 0.9]$ and $x \in [0.8, 0.801]$ (right)

intermediate data approximation at the boundary: This may generate a strong reflecting wave, which is always nonphysical when the free boundary conditions are used.

Notice that such reflected waves and their interaction with the waves present inside the computational domain can be observed not only in this example, but in the 2-D Example 4 as well.

Example 2—Stationary Contact Wave, Traveling Shock, and Rarefaction Wave

In the second example taken from [7], the initial conditions,

$$\big(\rho(x,0), u(x,0), p(x,0)\big) = \begin{cases} (1, -19.59745, 1000) & \text{if } x < 0.8, \\ (1, -19.59745, 0.01) & \text{otherwise,} \end{cases}$$

are prescribed in the computational domain [0, 1] subject to the free boundary conditions.

We compute the numerical solutions until the final time $t = 0.012$ using both the NEW and OLD schemes on two uniform meshes, the coarse and fine ones with $\Delta x = 1/200$ and $1/8000$, respectively. The numerical results, plotted in Figure 3, show that the NEW and OLD schemes achieve similar resolutions of both shock and contact waves. At the same time, the numerical results computed by the NEW scheme is non-oscillatory, while the OLD scheme solutions contain small oscillations, whose magnitude does not decay when the mesh is refined.

Example 3—2-D Riemann Problem

In the first 2-D example, we consider Configuration 3 of the 2-D Riemann problems taken from [9]; see also [14, 15, 21]. The initial conditions,

$$(\rho(x,y,0), u(x,y,0), v(x,y,0), p(x,y,0)) = \begin{cases} (1.5, 0, 0, 1.5), & x > 1,\ y > 1, \\ (0.5323, 1.206, 0, 0.3), & x < 1,\ y > 1, \\ (0.138, 1.206, 1.206, 0.029), & x < 1,\ y < 1, \\ (0.5323, 0, 1.206, 0.3), & x > 1,\ y < 1, \end{cases}$$

are prescribed in the computational domain $[0, 1.2] \times [0, 1.2]$ subject to the free boundary conditions. We compute the solution using both the NEW and OLD schemes on a uniform

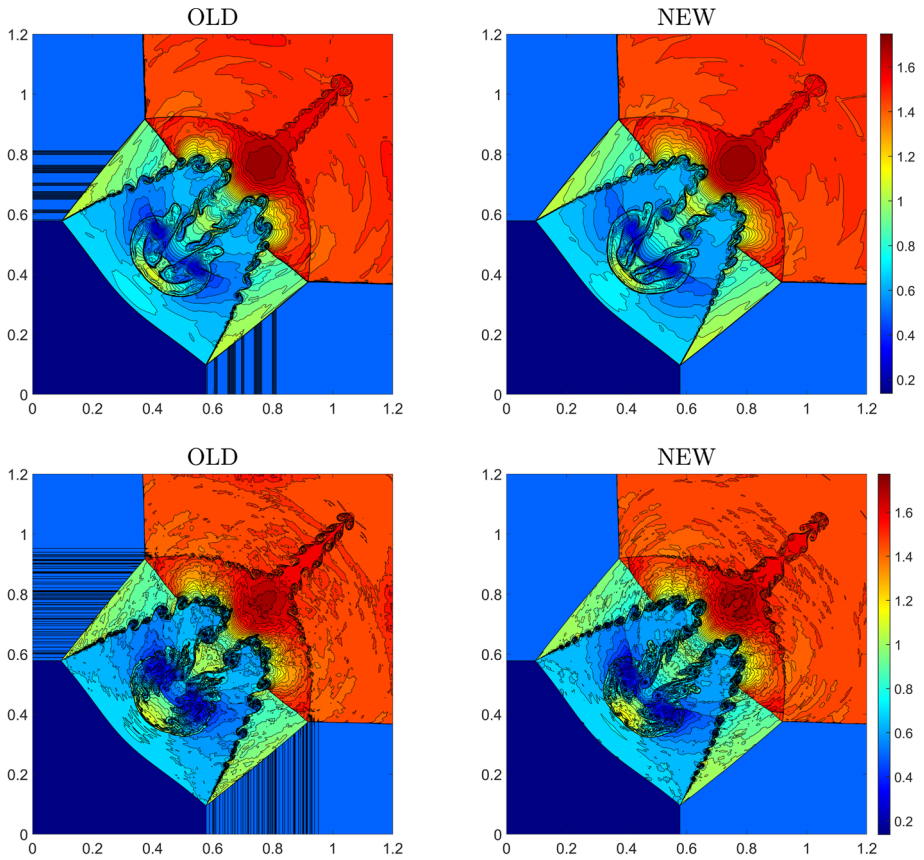

Fig. 4 Example 3: Density (ρ) computed by the OLD (left column) and NEW (right column) schemes on the uniform meshes with $\Delta x = \Delta y = 1/1250$ (top row) and $\Delta x = \Delta y = 1/5000$ (bottom row)

mesh with $\Delta x = \Delta y = 1/1250$ until the final time $t = 1$ and present the obtained densities in Figure 4 (top row). As one can see, the NEW solution is substantially less oscillatory than the OLD one, and the resolution achieved by the NEW and OLD schemes seems to be comparable. It is instructive to check whether there are still oscillations in the solution computed by the OLD scheme on finer meshes. To this end, we refine the mesh to $\Delta x = \Delta y = 1/5000$. The obtained numerical results are plotted in Figure 4 (bottom row), where one can clearly see that the solution computed by the OLD scheme is still substantially more oscillatory than the NEW scheme solution.

Example 4—Explosion Problem

In this example, we consider the explosion problem taken from [12] with the following initial conditions:

$$(\rho(x, y, 0), u(x, y, 0), v(x, y, 0), p(x, y, 0)) = \begin{cases} (1, 0, 0, 1), & x^2 + y^2 < 0.16, \\ (0.125, 0, 0, 0.1), & \text{otherwise}, \end{cases}$$

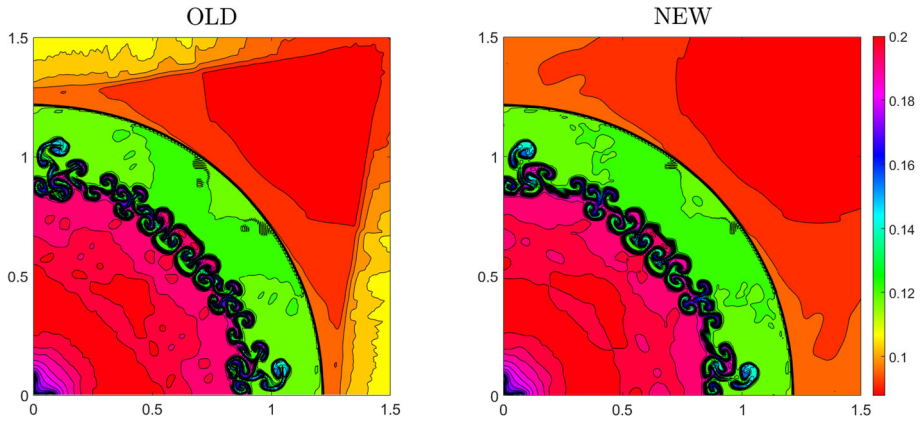

Fig. 5 Example 4: Density (ρ) computed by the OLD (left) and NEW (right) schemes

which are prescribed in the computational domain $[0, 1.5] \times [0, 1.5]$ subject to the solid wall boundary conditions at $x = 0$ and $y = 0$ and free boundary conditions at $x = 1.5$ and $y = 1.5$.

We compute the solution using the NEW and OLD schemes on a uniform mesh with $\Delta x = \Delta y = 3/800$ until the final time $t = 3.2$. The obtained densities are presented in Figure 5, where one can clearly see that there are obvious oscillations along the boundaries $x = 1.5$ and $y = 1.5$ in the numerical results computed by the OLD scheme, while the oscillations are substantially smaller in the numerical results computed by the NEW scheme. At the same time, in this example, the OLD scheme achieves a slightly better resolution.

Example 5—Implosion Problem In the last example, we test the implosion problem also taken from [12]. The initial conditions,

$$(\rho(x, y, 0), u(x, y, 0), v(x, y, 0), p(x, y, 0)) = \begin{cases} (0.125, 0, 0, 0.14), & |x| + |y| < 0.15, \\ (1, 0, 0, 1), & \text{otherwise}, \end{cases}$$

are prescribed in the computational domain $[0, 0.3] \times [0, 0.3]$ subject to the solid wall boundary conditions.

We compute the solution using the NEW and OLD schemes on a uniform mesh with $\Delta x = \Delta y = 1/2000$ until the final time $t = 2.5$. The obtained densities are presented in Figure 6. As one can see, the jet generated by the NEW scheme propagates to a larger extent than the jet produced by the OLD scheme, which demonstrates that in this example, the NEW scheme achieves slightly higher resolution than the OLD scheme.

Remark 3.2 We would like to point out that the proposed new LDCU scheme is semi-discrete and one can use different time discretizations—not necessarily SSPRK3 one. Instead one may obtain a second-order fully discrete scheme though a substantially more efficient MUSCL-Hancock-type framework briefly described in Appendix A. To perform a "fair" comparison between the SSPRK3 and MUSCL-Hancock approaches, we measure the CPU time consumed by the NEW scheme in Example 5 and refine the mesh used by the MUSCL-Hancock-type scheme (with the same CFL number 0.475) that exactly the same CPU time is consumed by both of the compared schemes. The corresponding finer mesh is of size $\Delta x = \Delta y = 1/2400$ for the MUSCL-Hancock-type scheme. The obtained MUSCL-

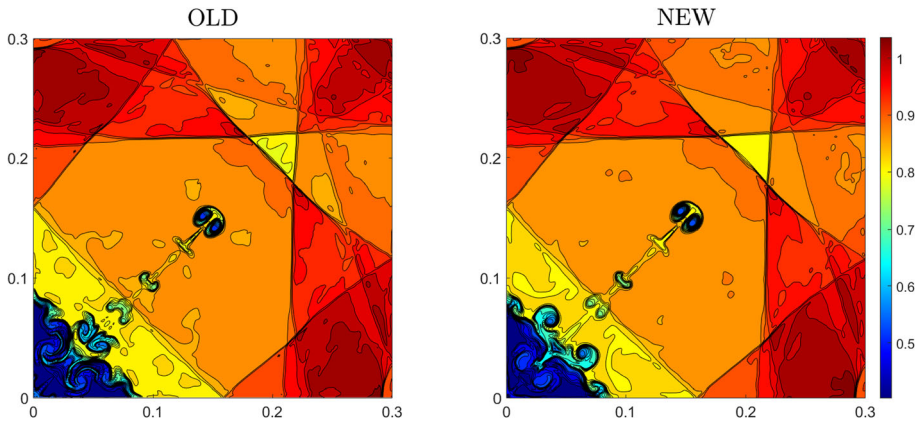

Fig. 6 Example 5: Density (ρ) computed by the OLD (left) and NEW (right) schemes on the uniform mesh with $\Delta x = \Delta y = 1/2000$

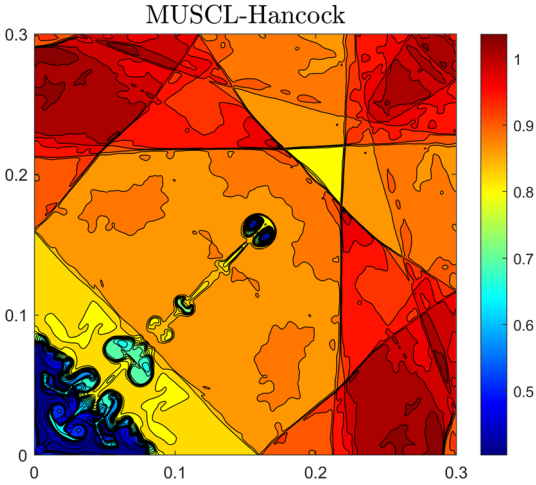

Fig. 7 Example 5: Density (ρ) computed by the new LDCU scheme combined with the MUSCL-Hancock approach for time discretization using $\Delta x = \Delta y = 1/2400$. Notice that this result was computed within the same CPU time as the solution shown in Figure 6 (right)

Hancock results are plotted in Figure 7, where one can see that the MUSCL-Hancock-based new LDCU scheme achieves higher resolution than the SSPRK3-based one.

Even though the MUSCL-Hancock approach seems to be more efficient than the SSPRK3 one, it has stability issues related to the positivity preservation of computed ρ and p. Note that it has been recently proved in [3] that the new LDCU schemes combined with explicit SSP ODE solvers can be made positivity preserving (PP) by using a special PP reconstruction and by a slight modification of the 2-D LDCU numerical fluxes (the 1-D LDCU flux does not need to be changed to enforce provably PP property). However, if the MUSCL-Hancock approach is used, much more substantial modifications (see [18]) are to be made to ensure that the resulting scheme is PP. In addition, the CFL number in the latter case should be substantially reduced [18], which would inevitably affect the efficiency of the MUSCL-Hancock approach.

4 Conclusion

In this paper, we have proposed a very simple but systematic modification of the low-dissipation central-upwind (LDCU) schemes. The developed new LDCU schemes are more accurate and stable than the original ones. A better stability of the new LDCU schemes can be clearly seen near the boundaries where the original LDCU schemes often produce large spurious oscillations. The new schemes have been applied to the one- and two-dimensional Euler equations of gas dynamics and were tested on a number of numerical examples, which clearly demonstrate that they outperform the original LDCU schemes.

We would also like to point out that the new LDCU schemes have been already successfully applied to the multifluid compressible Euler equations in the [2], and we plan to apply them to a variety of challenging hyperbolic systems of nonlinear PDEs in the future work. To this end, we will need to understand how the available degrees of freedom can be used to better approximate the solution of the system at hand at the projection step.

A 2-D MUSCL-Hancock Discretization

In this appendix, we briefly describe a 2-D version of the MUSCL-Hancock approach originally introduced in [20].

We begin by reconstructing the point values $\boldsymbol{U}^{n,\mp}_{j\pm\frac{1}{2},k}$ and $\boldsymbol{U}^{n,\mp}_{j,k\pm\frac{1}{2}}$ at a certain time level $t = t^n$ (computed in the same way as $\boldsymbol{U}^{\mp}_{j\pm\frac{1}{2},k}$ and $\boldsymbol{U}^{\mp}_{j,k\pm\frac{1}{2}}$ have been computed in §2.3), which are then advanced to the time level $t = t^{n+\frac{1}{2}} := t^n + \Delta t^n/2$ by

$$\begin{aligned}
\boldsymbol{U}^{n+\frac{1}{2},-}_{j+\frac{1}{2},k} &:= \boldsymbol{U}^{n,-}_{j+\frac{1}{2},k} - \frac{\Delta t^n}{2\Delta x}\Big[\boldsymbol{F}\big(\boldsymbol{U}^{n,-}_{j+\frac{1}{2},k}\big) - \boldsymbol{F}\big(\boldsymbol{U}^{n,+}_{j-\frac{1}{2},k}\big)\Big] - \frac{\Delta t^n}{2\Delta y}\Big[\boldsymbol{G}\big(\boldsymbol{U}^{n,-}_{j,k+\frac{1}{2}}\big) - \boldsymbol{G}\big(\boldsymbol{U}^{n,+}_{j,k-\frac{1}{2}}\big)\Big],\\
\boldsymbol{U}^{n+\frac{1}{2},+}_{j-\frac{1}{2},k} &:= \boldsymbol{U}^{n,+}_{j-\frac{1}{2},k} - \frac{\Delta t^n}{2\Delta x}\Big[\boldsymbol{F}\big(\boldsymbol{U}^{n,-}_{j+\frac{1}{2},k}\big) - \boldsymbol{F}\big(\boldsymbol{U}^{n,+}_{j-\frac{1}{2},k}\big)\Big] - \frac{\Delta t^n}{2\Delta y}\Big[\boldsymbol{G}\big(\boldsymbol{U}^{n,-}_{j,k+\frac{1}{2}}\big) - \boldsymbol{G}\big(\boldsymbol{U}^{n,+}_{j,k-\frac{1}{2}}\big)\Big],\\
\boldsymbol{U}^{n+\frac{1}{2},-}_{j,k+\frac{1}{2}} &:= \boldsymbol{U}^{n,-}_{j,k+\frac{1}{2}} - \frac{\Delta t^n}{2\Delta x}\Big[\boldsymbol{F}\big(\boldsymbol{U}^{n,-}_{j+\frac{1}{2},k}\big) - \boldsymbol{F}\big(\boldsymbol{U}^{n,+}_{j-\frac{1}{2},k}\big)\Big] - \frac{\Delta t^n}{2\Delta y}\Big[\boldsymbol{G}\big(\boldsymbol{U}^{n,-}_{j,k+\frac{1}{2}}\big) - \boldsymbol{G}\big(\boldsymbol{U}^{n,+}_{j,k-\frac{1}{2}}\big)\Big],\\
\boldsymbol{U}^{n+\frac{1}{2},+}_{j,k-\frac{1}{2}} &:= \boldsymbol{U}^{n,+}_{j,k-\frac{1}{2}} - \frac{\Delta t^n}{2\Delta x}\Big[\boldsymbol{F}\big(\boldsymbol{U}^{n,-}_{j+\frac{1}{2},k}\big) - \boldsymbol{F}\big(\boldsymbol{U}^{n,+}_{j-\frac{1}{2},k}\big)\Big] - \frac{\Delta t^n}{2\Delta y}\Big[\boldsymbol{G}\big(\boldsymbol{U}^{n,-}_{j,k+\frac{1}{2}}\big) - \boldsymbol{G}\big(\boldsymbol{U}^{n,+}_{j,k-\frac{1}{2}}\big)\Big].
\end{aligned} \tag{A.1}$$

Finally, the solution at the new time level $t = t^{n+1} := t^n + \Delta t^n$ is obtained by

$$\overline{\boldsymbol{U}}^{n+1}_{j,k} = \overline{\boldsymbol{U}}^{n}_{j,k} - \frac{\Delta t^n}{\Delta x}\Big(\boldsymbol{\mathcal{F}}^{n+\frac{1}{2}}_{j+\frac{1}{2},k} - \boldsymbol{\mathcal{F}}^{n+\frac{1}{2}}_{j-\frac{1}{2},k}\Big) - \frac{\Delta t^n}{\Delta y}\Big(\boldsymbol{\mathcal{G}}^{n+\frac{1}{2}}_{j,k+\frac{1}{2}} - \boldsymbol{\mathcal{G}}^{n+\frac{1}{2}}_{j,k-\frac{1}{2}}\Big),$$

where $\boldsymbol{\mathcal{F}}^{n+\frac{1}{2}}_{j+\frac{1}{2},k}$ and $\boldsymbol{\mathcal{G}}^{n+\frac{1}{2}}_{j,k+\frac{1}{2}}$ represents the x- and y-numerical fluxes computed at the time level $t^{n+\frac{1}{2}}$ using the values predicted in (A.1).

Funding The work of S. Chu was supported in part by the DFG (German Research Foundation) through HE5386/19-3, 27-1. The work of A. Kurganov was supported in part by NSFC grant 12171226, and by the fund of the Guangdong Provincial Key Laboratory of Computational Science and Material Design (No. 2019B030301001).

Data Availability The data that support the findings of this study and FORTRAN codes developed by the authors and used to obtain all of the presented numerical results are available from the corresponding author upon reasonable request.

Declarations

Conflicts of Interest On behalf of all authors, the corresponding author states that there is no conflict of interest.

References

1. Chertock, A., Chu, S., Herty, M., Kurganov, A., Lukáčová-Medvid'ová, M.: Local characteristic decomposition based central-upwind scheme, J. Comput. Phys., 473 Paper No. 111718 (2023)
2. Chu, S., Kurganov, A., Xin, R.: Low-dissipation central-upwind schemes for compressible multifluids, J. Comput. Phys., 518 Paper No. 113311 (2024)
3. Cui, S., Gu, Y., Kurganov, A., Wu, K., Xin, R.: Positivity-preserving new low-dissipation central-upwind schemes for compressible Euler equations, Submitted. Preprint available at https://ssrn.com/abstract=5023460
4. Gottlieb, S., Ketcheson, D., Shu, C.-W.: Strong stability preserving Runge-Kutta and multistep time discretizations, World Scientific Publishing Co. Pte. Ltd., Hackensack, NJ (2011)
5. Gottlieb, S., Shu, C.-W., Tadmor, E.: Strong stability-preserving high-order time discretization methods. SIAM Rev. **43**, 89–112 (2001)
6. Kuganov, A., Noelle, S., Petrova, G.: Semidiscrete central-upwind schemes for hyperbolic conservation laws and Hamilton-Jacobi equations. SIAM J. Sci. Comput. **23**, 707–740 (2001)
7. Kurganov, A., Lin, C.-T.: On the reduction of numerical dissipation in central-upwind schemes, Commun. Comput. Phys. **2**, 141–163 (2007)
8. Kurganov, A., Tadmor, E.: New high-resolution semi-discrete central schemes for Hamilton-Jacobi equations. J. Comput. Phys. **160**, 720–742 (2000)
9. Kurganov, A., Tadmor, E.: Solution of two-dimensional Riemann problems for gas dynamics without Riemann problem solvers. Numer. Methods Partial Differential Equations **18**, 584–608 (2002)
10. Kurganov, A., Xin, R.: New low-dissipation central-upwind scheme, J. Sci. Comput., 96 Paper No. 56 (2023)
11. Lie, K.-A., Noelle, S.: On the artificial compression method for second-order nonoscillatory central difference schemes for systems of conservation laws. SIAM J. Sci. Comput. **24**, 1157–1174 (2003)
12. Liska, R., Wendroff, B.: Comparison of several difference schemes on 1D and 2D test problems for the Euler equations. SIAM J. Sci. Comput. **25**, 995–1017 (2003)
13. Nessyahu, H., Tadmor, E.: Nonoscillatory central differencing for hyperbolic conservation laws. J. Comput. Phys. **87**, 408–463 (1990)
14. Schulz-Rinne, C.W.: Classification of the Riemann problem for two-dimensional gas dynamics. SIAM J. Math. Anal. **24**, 76–88 (1993)
15. Schulz-Rinne, C.W., Collins, J.P., Glaz, H.M.: Numerical solution of the Riemann problem for two-dimensional gas dynamics. SIAM J. Sci. Comput. **14**, 1394–1414 (1993)
16. Shu, C.-W., Osher, S.: Efficient implementation of essentially non-oscillatory shock-capturing schemes. J. Comput. Phys. **77**, 439–471 (1988)
17. Sweby, P.K.: High resolution schemes using flux limiters for hyperbolic conservation laws. SIAM J. Numer. Anal. **21**, 995–1011 (1984)
18. Tong, W., Yan, R., Chen, G.: A class of bound-preserving MUSCL-Hancock schemes in two dimensions, J. Comput. Phys., 498 Paper No. 112668 (2024)
19. van Leer, B.: Towards the ultimate conservative difference scheme. V. A second-order sequel to Godunov's method, J. Comput. Phys., 32 pp. 101–136 (1979)
20. van Leer, B.: On the relation between the upwind-differencing schemes of Godunov, Engquist-Osher and Roe. SIAM J. Sci. Stat. Comput. **5**, 1–20 (1984)
21. Zheng, Y.: Systems of conservation laws: Two-dimensional Riemann problems, Progress in Nonlinear Differential Equations and their Applications, 38. Birkhäuser Boston Inc, Boston, MA (2001)